Palaeogeography, Palaeoclimatology, Palaeoecology 598 (2022) 111016

Contents lists available at ScienceDirect

Palaeogeography, Palaeoclimatology, Palaeoecology

journal homepage: www.elsevier.com/locate/palaeo

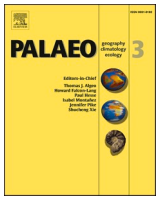

Soil salt and microbiome diversification over the past 3700 million years

Gregory J. Retallack

Department of Earth Sciences, University of Oregon Eugene, Oregon 97403, USA

ARTICLE INFO

Editor: Shucheng Xie

Keywords:
Paleosol
Paleoproductivity
Atmospheric CO_2
Atmospheric O_2
Plant evolution

ABSTRACT

A geological history of pedogenic salts and their microbiomes can now be reconstructed from a review of thousands of described paleosols ranging in age back 3700 Ma. The current diversity of evaporite minerals within paleosol gypsic (By) horizons may have begun with kieserite ($MgSO_4.H_2O$ at 3700 Ma), then barite ($BaSO_4$ at 3458 Ma), and gypsum ($CaSO_4.2H_2O$ at 3217 Ma). Pedogenic carbonate of calcic (Bk) horizons appeared later, first nahcolite ($NaHCO_3$ at 3016 Ma), then dolomite ($(Mg,Ca)(CO_3)_2$ at 2403 Ma), and low-magnesium calcite ($CaCO_3$ at 1460 Ma). The earliest occurrence of each salt is shallow in paleosol profiles (12–25 cm), but deeper (50–100 cm) salt horizons (By and Bk) horizons appear later in the Proterozoic and Paleozoic. These changes can be normalized for estimated differences in mean annual precipitation in the same paleosol from both depth to salts and from chemical composition, which demonstrated that depth to salts and soil productivity measured as respired carbon dioxide showed unchanged relationship with mean annual precipitation in deep time. Stepwise increases in soil respiration through time inferred from depth of soil salts reflects evolving soil microbiomes and atmospheric composition cued to major advances in the evolution of life on land, such as the evolution of anaerobic, then aerobic photosynthetic microbes, then land plants, and trees.

1. Introduction

Salts are simple compounds of a cation and an anion formed by precipitation from solution, mainly in aridland soils (Table 1). Their solubility reflects degree of soil aridity from dolomite to calcite (both Bk horizon), gypsum (By horizon), and then to mirabilite and thenardite (both Bz) in hyperarid soils (Retallack, 2019). Salts in soils not only reflect soil chemistry and climate, but a diversity of vegetation and microbiomes. For example, deserts of southwestern Australia have mulga shrubland (*Acacia aneura*) on lateritic residual soils without soluble salts, as well as mallee woodland (*Eucalyptus salubris*) on calcareous nodular soils (Anand and Paine, 2002), and lightly vegetated salt pans within the same small areas (Benison and Bowen, 2015). The gypsiferous, dysaerobic salt pans have a distinctive microbiome rich in sulfur oxidizing bacteria and actinobacteria (Mormile et al., 2009), unlike proteobacterial-cyanobacterial-eukaryotic microbiomes of nearby aerobic calcareous (Benison and Bowen, 2015) and lateritic soils (O'Brien et al., 2019). The gypsiferous soils are also analogs for Martian (Mormile et al., 2009; Retallack, 2014) and Archean paleosols rich in sulfate minerals (Nabhan et al., 2016; Retallack et al., 2016; Retallack and Noffke, 2019). The deeply weathered lateritic soils also have Precambrian analogs on major geological unconformities (Beaty and Planavsky, 2020). This modern soil diversity is the result of evolutionary diversification of life on land, which is here traced in the long fossil record of paleosols.

This study of soil salts and microbiomes in deep time is based on a compilation of 7342 previously published paleosols (see Supplementary Information Online Table S1). Only paleosols with soluble salts were included, despite an additional record of Precambrian paleosols without salts (Rye and Holland, 1990), which also has evidence of microbial life back at least 3 Ga from alumina enrichment and phosphate depletion (Neaman et al., 2005; Beaty and Planavsky, 2020). Paleosols with soil salts provide evidence of Eh, pH, and other environmental variables that control composition of the soil microbiome and microbial productivity (Mormile et al., 20099; Breecker and Retallack, 2014; Benison and Bowen, 2015). This compiled record is one of ancient aridlands, regions with excess evaporation over precipitation, allowing soil salts to accumulate within the soil at the fringe of biological activity. This is not a simple leaching process, but one of mobilization followed by precipitation within a definite horizon (Monger et al., 1991; Breecker et al., 2009). Soil salts are recognized in paleosols by the same criteria as in modern soils: they form subsurface horizons of nodules or sand crystals (Fig. 1-2) with replacive petrographic textures (Fig. 2), and commonly in spherulitic "desert roses" (Nabhan et al., 2016; Retallack et al., 2016; Retallack, 2018). Similar gypsum and barite desert roses are widely documented in modern soils (Traveria et al., 1971; Carson et al., 1982;

E-mail address: gregr@uoregon.edu.

https://doi.org/10.1016/j.palaeo.2022.111016
Received 23 November 2021; Received in revised form 7 April 2022; Accepted 24 April 2022
Available online 28 April 2022

Table 1
Salts known from paleosols.

Name	Chemical formula	Crystal form
anhydrite	$CaSO_4$	orthorhombic cubic
barite	$BaSO_4$	orthorhombic tabular
bassanite	$CaSO_4.12H_2O$	monoclinic needles
calcite	$CaCO_3$	trigonal rhombohedral to micrite
dolomite	$(Mg,Ca)(CO_3)_2$	trigonal rhombohedral to micrite
gypsum	$CaSO_4.2H_2O$	monoclinic tabular, fishtail twins
kieserite	$MgSO_4.H_2O$	monoclinic granular
mirabilite	$NaSO_4.10H_2O$	monoclinic needles
nahcolite	$NaHCO_3$	monoclinic pseudohexagonal prisms
thenardite	$NaSO_4$	monoclinic dipyramidal

Al-Kofahi et al., 1993; Lock, 2002; Jennings and Driese, 2014). Especially soluble salts such as gypsum are prone to dissolution, but can be identified by crystal form of pseudomorphous replacements, and by microprobe analyses of internal remnants (Fig. 4). Evidence of a role for microbes in their formation comes from associated microfossils and pyrite framboids (Retallack et al., 2016), and for carbonates, isotopically light and highly correlated $\delta^{13}C$ and $\delta^{18}O$ values from decay of rubisco-fractionated isotopologues of CO_2 used to synthesize organic matter (Retallack, 2016; Broz et al., 2021).

2. Background to salts in soils and paleosols

A variety of salts form conspicuous horizons of nodules or desert roses in subsurface horizons of soils and paleosols, especially calcite, dolomite, gypsum and barite (Table 1). Nodules are massive fine-grained, hard, lumps, cemented by salts (Fig. 1). Desert roses are poikilotopic (with many included grains) crystals, but the salt cement retains optical continuity, and a distinct crystal outline (Fig. 2A-D). Desert roses and nodules of soils and paleosols are replacive and cementing (Fig. 3A, D-E), not displacive like limpid gypsum precipitated in saturated marine clays (Stefano et al., 2010; Ziegenbalg et al., 2010), or saline lakes (Benison and Goldstein, 2000; Benison and Bowen, 2015). Also limpid with few inclusions are aragonite crystals from springs as old as the Archean (Jones, 2017; Otálora et al., 2018). Less common in soils and paleosols (Fig. 2E-F, 3B) are small needles of thenardite, mirabilite, and kieserite at the soil surface, and in near-surface vugs and cracks (Whittig and Janitzky, 1963; Smykatz-Kloss and Roy, 2010; Stoker et al., 2011; Mees and Tursina, 2018; Diaz et al., 2020).

Salt minerals are soluble, and may only be preserved within rocks as silica or other pseudomorphs (Fig. 3C-D, F-G). The original salt can be inferred from crystallographic axes of preserved crystal faces (Buick and Dunlop, 1990; Lowe and Worrell, 1999), or distinctive features such as former anhydrite cubes, within former gypsum rhombs (Fig. 3F). There has been some debate about the original salt of Archean sand crystal pseudomorphs, as if only one kind of mineral is likely (Otálora et al., 2018), but Archean paleosols had several kinds of salts, like modern soils (Retallack et al., 2016; Retallack, 2018). Chemical analysis by ion microprobe can also provide maps of mineral abundance, such as the metamorphic mineral ripidolite $[(Mg,Fe,Al)_6(Si,Al)_4O_{10}(OH)_8]$ found in a highly metamorphosed paleosol (Fig. 4A). In that case the original monoclinic crystals were interpreted as sand-crystals of kieserite (Retallack and Noffke, 2019). In other cases, microprobe mapped residues of Ca or Ba in silica-replaced sand crystals (Fig. 4B-C) can be used to decide between former gypsum or barite (Retallack and Mao, 2019). Barite is common in Archean paleosols (Retallack et al., 2016; Retallack, 2018), which is surprising considering its rarity, very low solubility, and

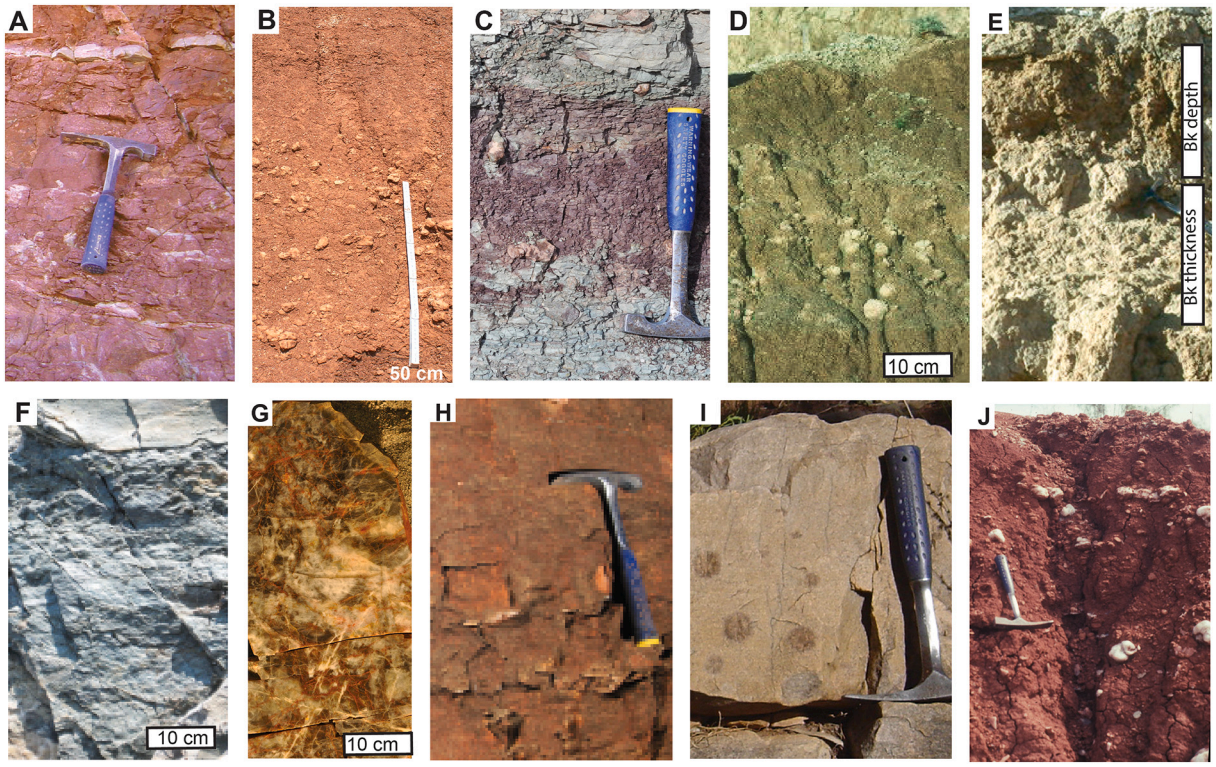

Fig. 1. Examples of Calcid (A-E) and Gypsid (F-J) paleosols: A, Mesoproterozoic (1460 Ma) Lyons pedotype from Spokane Formation near Wolf Creek, Montana (Winston and Link, 1993); B, Late Permian (253 Ma) "type A paleosol" from Bovevaya Gora, Russia (Kearsey et al., 2012); C, early Triassic (250 Ma) Kuta pedotype from Bethulie, South Africa (Retallack, 2021a); D, Oligocene Wisangie pedotype Badlands National Park, South Dakota (Retallack, 1983); E, late Miocene (7.5 Ma) Tatas pedotype near Dayville Oregon (Retallack et al., 2002); F, Archean (3700 Ma) Isi pedotype near Isukasia, Greenland (Retallack and Noffke, 2019); G, Archean (3459 Ma) Jurl pedotype from Panorama Portal, Western Australia (Retallack, 2018); H, Tonian (706 Ma) Alkynge pedotype from Ellery Creek, Northern Territory, Australia (Retallack, 2021b); I, Ediacaran (550 Ma) Muru pedotype from Brachina Gorge, South Australia (Retallack, 2013), J, Early Permian (281 Ma) paleosol from near Gillibrand, Texas (Retallack and Huang, 2010).

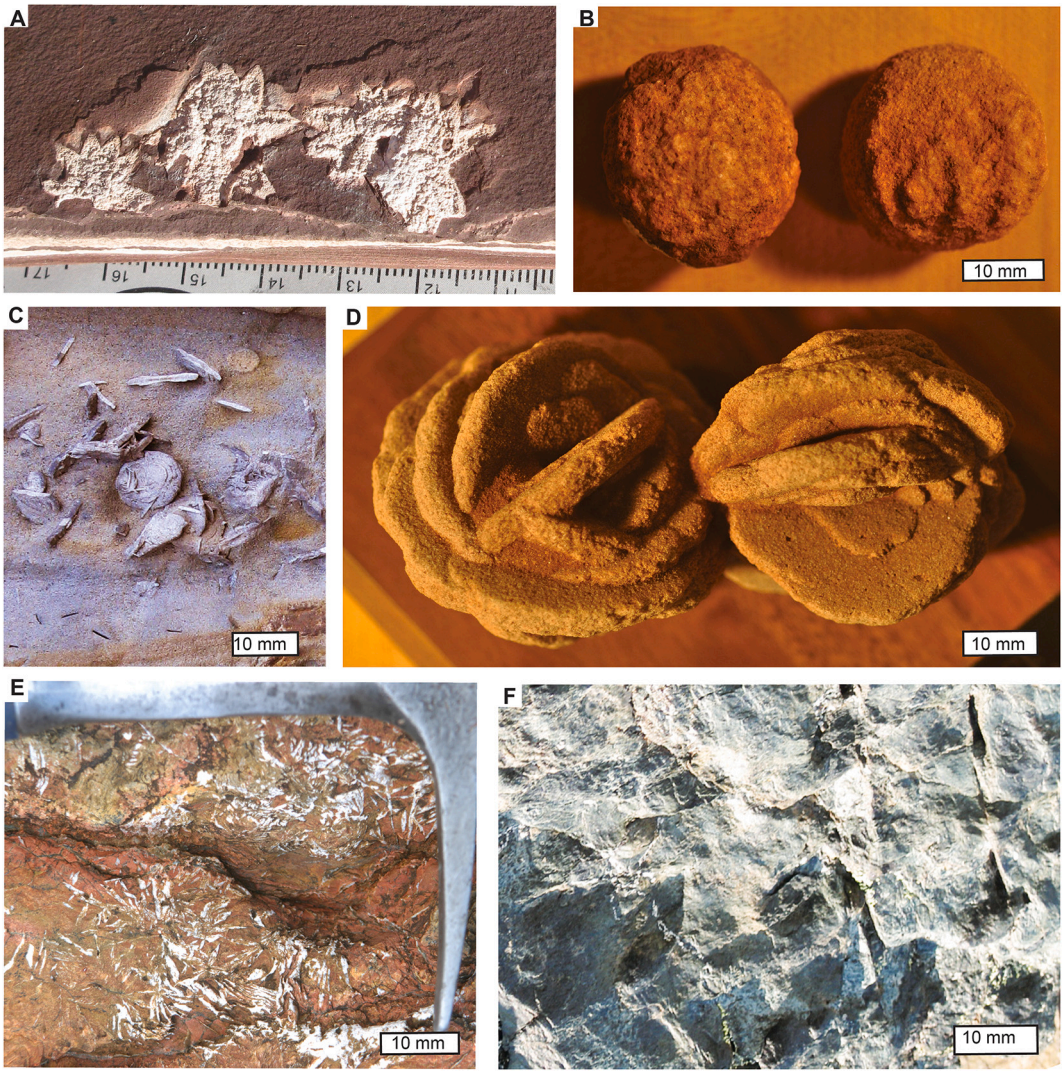

Fig. 2. Desert roses (A-D) and crystals (*E*-F) in hand specimens of paleosols: A, clay pseudomorph of gypsum desert rose from By horizon of Thamberalg pedotype in Ediacaran (599 Ma) Ranford Formation, Donkey Creek, Western Australia (Retallack, 2020); B, silica pseudomorphs of gypsum desert roses in By horizon of Muru pedotype from Ediacaran (547 Ma) Ediacara Member in Brachina Gorge, South Australia (Retallack, 2013); C, barite desert roses from Oligocene (20 Ma) Rockenberg Formation near Rockenberg, Germany (Dietrich, 1975); D, barite desert roses from By horizon of Early Permian (270 Ma) Garber Sandstone near Cimarron City, Oklahoma (Retallack, 2005b); E, silica pseudomorphs of mirabilite in A horizon of Viku pedotype from Cryogenian (640 Ma) Reynella Siltstone Member Hallett Cove, South Australia (Retallack et al., 2015); F, ripidolite pseudomorphs of kieserite in By horizon of Isi pedotype from Archean (3700 Ma) Isua Greenstone near Isukasia, Greenland (Retallack and Noffke, 2019). Specimens in Condon Collection of Museum of Natural and Cultural History, University of Oregon are (a), R4185 (b), F6345 (d), field photographs (c, e-f). (For interpretation of the references to colour in this figure legend, the reader is referred to the web version of this article.)

unusually low pH of mobilization in modern soils (Jennings and Driese, 2014).

Salts in soils form by desiccation and accumulate in climates with excess evaporation over precipitation (Fig. 5A: Smykatz-Kloss and Roy, 2010; Bockheim, 2014; Mees and Tursina, 2018). Life in soils also affects levels of water vapor and respired carbon dioxide, and thus modifies the effects of climate on depth at which salts can precipitate. Gypsum, calcite and dolomite all accumulate deeper within soils with higher biological productivity in more humid climates (Fig. 5B: Retallack, 2005a; Retallack and Huang, 2011; Breecker and Retallack, 2014).

Soil salts can be reprecipitated from parent materials, or from dust and alluvium reworked from gypsic and calcic soils within extensive desert basins (Quade et al., 2007). Sources of carbonate and sulfate also include atmospheric CO_2, SO_3 and SO_2 (Whittig and Janitzky, 1963; Ganzeveld et al., 1998; Breecker et al., 2009). Salt precipitation changed with the evolution of the atmosphere over geological time, with O_2 scarce in the atmosphere before 2.45 Ga, but CO_2, SO_3 and SO_2 more common before then (Hazen et al., 2008). While CO_2 in the atmosphere declined dramatically with the Devonian rise of land plants (Berner, 2006), CO_2 in soils increased with increased soil respiration fed by increased biomass of land plants (Retallack, 2022). Increased soil CO_2 may be responsible for the ecotone from gypsic to calcic soils in the Atacama Desert (Quade et al., 2007). Sulfur may also come from oxidation of pyrite and other sulfides (Jennings and Driese, 2014), and from evaporation of hypersaline water (Smykatz-Kloss and Roy, 2010; Stefano et al., 2010). The cations Ca^{2+}, Mg^{2+}, and Na^{+} come largely from dust of aridlands (Wang et al., 2012), but also from weathering of parent materials by weak carbonic acid at perineutral pH (Breecker et al., 2009), or by acid sulfate weathering of strong sulfuric acid at low pH (Benison and Bowen, 2015).

Nevertheless, gypsic and calcic soils form widely on extensive non-sulfurous and non-carbonate sedimentary parent materials of both playa lake basins and well drained desert soils of alluvial fans (Schlesinger, 1985; Harden et al., 1991), and biogenically induced formation is apparent in many modern soils (Hazen et al., 2008; Jennings and Driese, 2014). The particular salts precipitated depends to some extent on

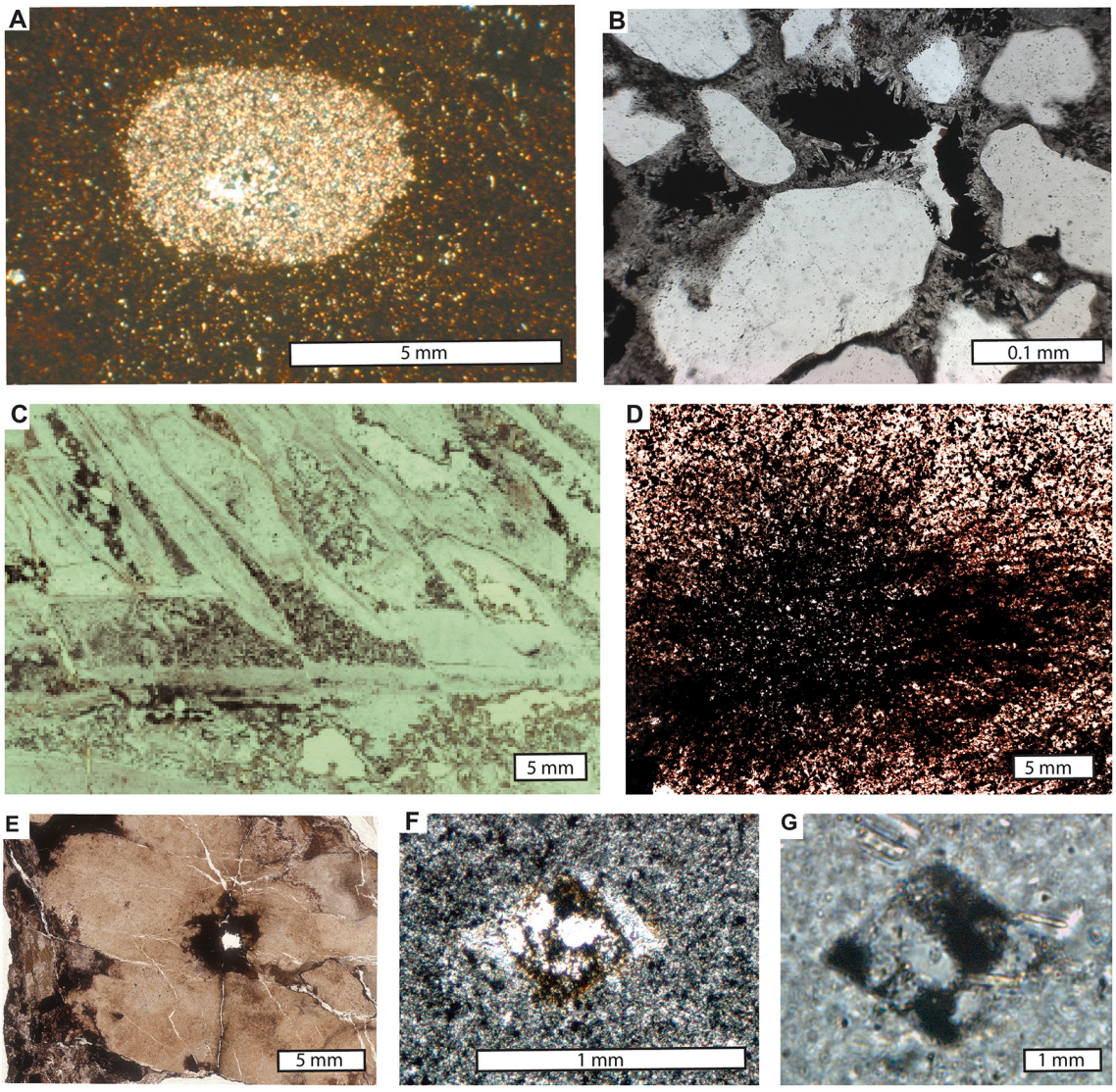

Fig. 3. Sand crystals (A, E) and pseudomorphs (B—D, F-G) in petrographic thin sections of paleosols: A, replacive poikilotopic micrite nodule in red siltstone of late Miocene (8.5 Ma) Bk horizon of Lal pedotype in Dhok Pathan Formation, Kaulial, Pakistan (Retallack, 1991); B, silica pseudomorphs of cavity-filling thenardite in A horizon of Dawaling pedotype in Paleoproterozoic (1738 Ma), Yunmengshan Formation near Daheitan, Henan, China; C, silica pseudomorphs of poikilotopic nahcolite crystals in By horizon of Kari pedotype in Archean (3016 Ma) Farrel Quartzite, Mt. Grant, Western Australia (Retallack et al., 2016); D, silica pseudomorph of gypsum desert rose from By horizon of Muru pedotype in Ediacaran (547 Ma) Ediacara Member in Brachina Gorge, South Australia (Retallack, 2013); E, gypsum desert rose from By horizon of Ekwatha pedotype in Tonian (770 Ma) Tanner Member, Nankoweap Creek, Arizona (Retallack et al., 2021a); F, poikilotopic cubic anhydrite within original monoclinic gypsum pseudomorph in By horizon of Nickerson pedotype Ediacaran (580 Ma) Squantum Member at Squantum, Massachusetts; G, pseudomorph of poikilotopic monoclinic gypsum in By horizon of Jurl pedotype in Archean (3458 Ma) Panorama Formation at Panorama Portal, Western Australia (Retallack, 2018). (For interpretation of the references to colour in this figure legend, the reader is referred to the web version of this article.)

particular microbiomes, such as sulfate favored by prokaryotic communities of sulfur-oxidizing bacteria and actinobacteria (Crits-Christoph et al., 2013). These sulfate-forming communities of hyperarid soils in the Atacama Desert pass laterally into arid communities of eukaryotic algae, amoebae, and lichens which create calcareous soils (Navarro-González et al., 2003; Neilson et al., 2017; Araya et al., 2020), in part from decay of lichen oxalate (Giordani et al., 2003; Vítek et al., 2013). Galactose and rhamnose from microbial extracellular polysaccharides (EPS) are catalytic for dolomite, and produced by methanogens, fermenting bacteria, and sulfur reducing bacteria under dysaerobic conditions (Zhang et al., 2012). In contrast, glucose and mannose EPS are catalytic for calcite, and produced by cyanobacteria, among others in well drained soils (Zhang et al., 2012). Fungi also promote calcite precipitation in soils (Monger et al., 1991). Thus, dolomite versus calcite precipitation is partly dependent on microbiomes encouraged by the CO_2/O_2 mixing ratio within soils, which is highest in soils and seasons of the year with high microbial respiration (Breecker et al., 2009).

3. Materials and methods

Key field measurements compiled for this study were depths to the salt horizon (Bk or By), thickness of the salt horizon, and size of nodules or sand crystals. The depth measured in paleosols in the field can be compared with modern soils after correction for burial compaction (C, fraction) calculated from depth of burial (B, km) by Eq. (1) in which 0.51, 0.49, and 0.27, are solidity, initial porosity and a fitting constant, respectively, for Aridisol soils (Sheldon and Retallack, 2001).

$$C = \frac{-0.51 \times 100}{\left\{\left(\frac{0.49}{e^{\frac{B}{0.27}}}\right) - 1\right\}} \quad (1)$$

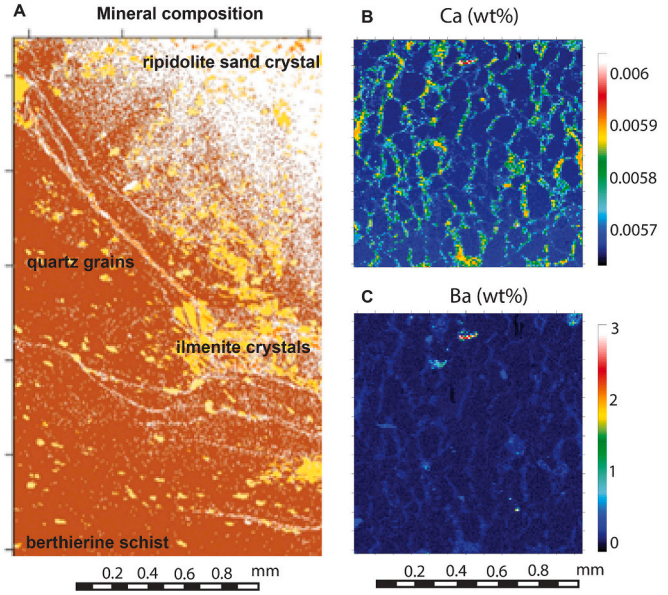

Fig. 4. Microprobe chemical mapping of sand crystals in paleosols: A, Archean (3700 Ma) By horizon of Isi pedotype from Isukasia, Greenland, modes calculated from 180,000 analyses (Retallack and Noffke, 2019); B—C, Paleoproterozoic (1900 Ma) By horizon of Kumbar pedotype, Stirling Range Formation, Barnett Peak, Western Australia, elemental abundances to discriminate gypsum from barite within poikilotopic crystal (Retallack and Mao, 2019).

Depth to gypsic (D_g, cm) and calcic (D_c, cm) horizons in soils are related to mean annual precipitation (P, mm), by Eq. (2) (from Retallack, 2005a, 2005b: $r^2 = 0.52$, s.e. $= \pm 147$, $p = 0.0001$) and 3 (from Retallack and Huang, 2010: $r^2 = 0.63$, s.e. $= \pm 129$, p = 0.0001). The relationship with gypsic and calcic horizons is similar in modern soils at salt depths of less than 120 cm, but gypsic horizons deeper than that are not known and calcic horizons are not deeper than 200 cm in soils under precipitation of more than 1000 mm (Fig. 5A).

$$P = 137.24 + 6.45D_c - 0.0132(D_c)^2 \quad (2)$$

$$P = 87.593e^{0.0209D_g} \quad (3)$$

Erosion in soils compromises these relationships, especially in soils of hillslopes and erosional landscapes (Royer, 1999). For this reason, Eqs. (2) and (3) were based only on Holocene soils of sedimentary parent materials in aggrading fluvial sedimentary settings, and applied to long sequences of alluvial sedimentary rocks (Retallack, 2005a, 2005b; Retallack and Huang, 2010). A few paleosols were flagged for erosion by overlying paleochannels or lack of converging root traces toward the surface (Retallack, 1983, 1992; Retallack et al., 1999). Depths to salts in long stratigraphic sequences show striking consistence and cycles of paleoclimate in stratigraphic successions (Retallack et al., 2004; Retallack, 2009).

Ecosystem variables such as primary productivity and respired soil CO_2 also increase with mean annual precipitation and depth to salts in soils (Fig. 5B). Seasonal variation in soil CO_2 is large, ranging from a peak during spring regrowth and a low in winter dormancy, but late growing season soil CO_2 is critical to late growing season precipitation of calcite and gypsum in soils (Breecker and Retallack, 2014). Depth to gypsic (D_g, cm) and calcic (D_c, cm) horizons in soils are empirically correlated with late growing season soil CO_2 (C_r, ppm), 2014), by Eq. (4) ($r^2 = 0.66$, s.e. $= \pm 768$, p = 0.0001) and 5 ($r^2 = 0.64$, s.e. $= \pm 552$, $p = 0.05$).

$$C_r = 25.3D_c + 588 \quad (4)$$

$$C_r = 42.9D_g + 399 \quad (5)$$

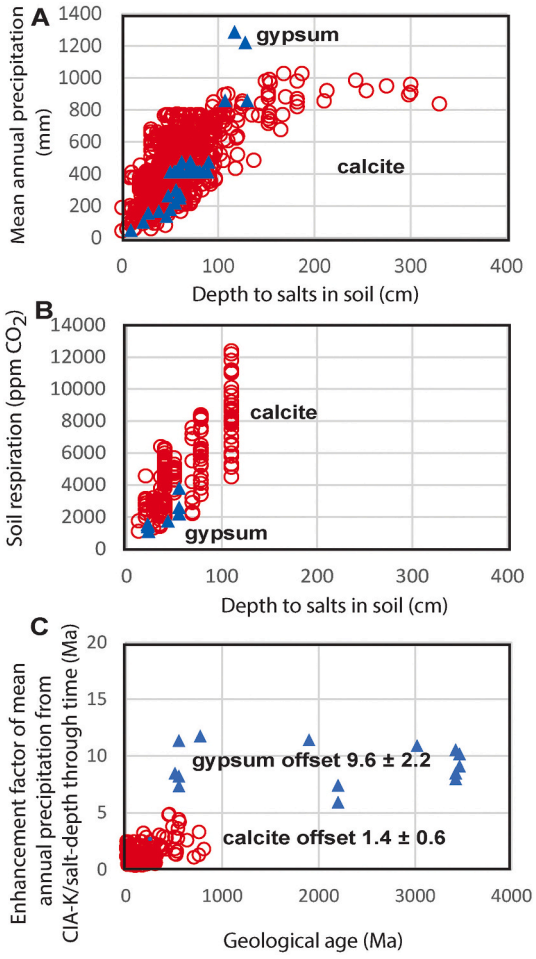

Fig. 5. Depth to salts in modern soils versus their mean annual precipitation (A) and soil respiration (B), and enhancement factor of estimates of mean annual precipitation from chemical weathering versus depth to salts through geological time (C).

4. Can modern climofunctions for soil salts be used in deep time?

Salts today precipitate in soils with moisture and acidity generated by soil respiration waning at the end of the growing season at a characteristic depth in soils for particular mean annual precipitation and correlated ecosystem productivity (Fig. 5A-B: Breecker and Retallack, 2014;). Whether that was also true in the geological past can be addressed from independent geochemical estimates for mean annual precipitation in paleosols, using chemical index of alteration without potash (I, in moles) and Eqs. (6) and (7) (from Sheldon et al., 2002: $r^2 = 0.72$, s.e. $= \pm 182$, p = 0.0001).

$$I = \frac{100mAl_2O_3}{mAl_2O_3 + mCaO + Na_2O} \quad (6)$$

$$P = 221.1e^{0.0197I} \quad (7)$$

Relevant data on paleosol salt depth and matrix chemical composition includes 181 calcic paleosols and 14 gypsic paleosols (see Supplementary Information Online Table S2). Calculations of mean annual precipitation from depth to salts (Eqs. (4), (5)) and chemical composition of lower A horizons of the same paleosols (Eqs. (6), (7)) show a characteristic offset: by a factor of 1.4 ± 0.6 for 181 calcic paleosols, and a factor of 9.6 ± 2.2 for 15 gypsic paleosols (Fig. 5C). This offset normalizes mean annual precipitation effects for different paleosols, and

does not change significantly back in time (Fig. 5B). These differences arise from weathering of the sedimentary parent material of the paleosols in their source terranes, and the different style of weathering of calcic and gypsic soils. The parent material effect from source terrains more deeply weathered than the North American CIA-K paleohyetometer makes chemical estimates of mean annual precipitation higher than those from depth to calcic and gypsic horizons. Unlike calcic paleosols weathered and precipitated from carbonic acid at perineutral pH (Breecker and Retallack, 2014), gypsic paleosols were formed by strong sulfuric acid at pH of 3–4 (Benison and Bowen, 2015). Calcic paleosol chemical composition overestimates mean annual precipitation by a little, but gypsic paleosol chemical composition overestimates mean annual precipitation by an order of magnitude due to strong acid. Neither the calcic nor gypsic offset of chemical versus depth estimate shows a significant trend in deep time, suggesting common cause for salt depth and soil respiration in mean annual precipitation. Calcic microbiomes were an increase in productivity over gypsic microbiomes, as can be observed in the Atacama Desert today (Navarro-González et al., 2003; Neilson et al., 2017; Araya et al., 2020). Thus, salt depths in paleosols are a potentially useful proxy for microbiome respiration in deep time (Fig. 5C) as in modern soils (Fig. 5B).

5. Order of salt appearance in soils

Hesperian paleosols on Mars (Retallack, 2014) and Archean paleosols on Earth (Retallack et al., 2016; Retallack, 2018; Retallack and Noffke, 2019) have abundant sulfate crystals and nodules (Fig. 1d). This was an unexpected discovery because other redox sensitive elements such as iron and manganese in these paleosols are evidence of atmospheric oxygen levels too low to oxidize sulfur to sulfate (Retallack et al., 2021b). Such low atmospheric oxidation left much sulfur in Archean paleosols as pyrite framboids and other sulfides, which then could be microbially oxidized to sulfate (Retallack et al., 2016). Furthermore, Archean marine rocks lack sulfate evaporites and have mass-independent isotopic differentiation of sulfur, indicating very low sulfate ion concentrations in the Archean ocean (Canfield and Farquhar, 2009). Gypsic paleosols of the 3016 Ma Farrel Quartzite of Western Australia also have permineralized microfossils, with carbon isotopic compositions and organic morphologies compatible with interpretation as sulfur-oxidizing bacteria, actinobacteria, and methanogens (Retallack et al., 2016). Sulfate may have been produced by hydrothermal sulfur disproportionation (Einaudi et al., 2003), but given lack of evidence for hydrothermal alteration from rare earth elements (Sugahara et al., 2010), and associated microfossils and framboids, sulfate in these paleosols more likely came from biological oxidation of anaerobic sulfur by bacterial photosynthesis (Retallack et al., 2016).

The most ancient pedogenic sulfate may have been kieserite, not preserved, but inferred from metamorphic pseudomorphs of ripidolite in a 3700 Ma paleosol from Greenland (Fig. 4a). Kieserite is also known from 3500 to 3200 Ma Martian paleosols (Retallack, 2014). Barite is next to appear, and widespread, in 3470 Ma paleosols in both Western Australia (Retallack, 2018) and South Africa (Lowe and Worrell, 1999). Gypsum is next to appear in 3.2 Ga paleosols in South Africa (Nabhan et al., 2016). Similar bassanite is known in 3700 Ma paleosols on Mars (Retallack, 2014).

The oldest known carbonate in paleosols is nahcolite documented in 3016 Ma paleosols from Western Australia (Retallack et al., 2016), but similar chert pseudomorphs from rocks as old as 3470 Ma in South Africa and Western Australia may also have been paleosols (Lowe and Worrell, 1999). Nahcolite forms in acidic and evaporitic playa lakes, often with gypsum (Howari et al., 2002; Lowenstein et al., 2017).

Dolomite may be the next carbonate to appear along with traces of calcite in 2600 Ma paleosols in South Africa (Watanabe et al., 2004), although that particular dolomite is in layers rather than replacive nodules, so is more likely marine or lacustrine than pedogenic carbonate. More convincing are dispersed dolomite nodules in 2403 Ma

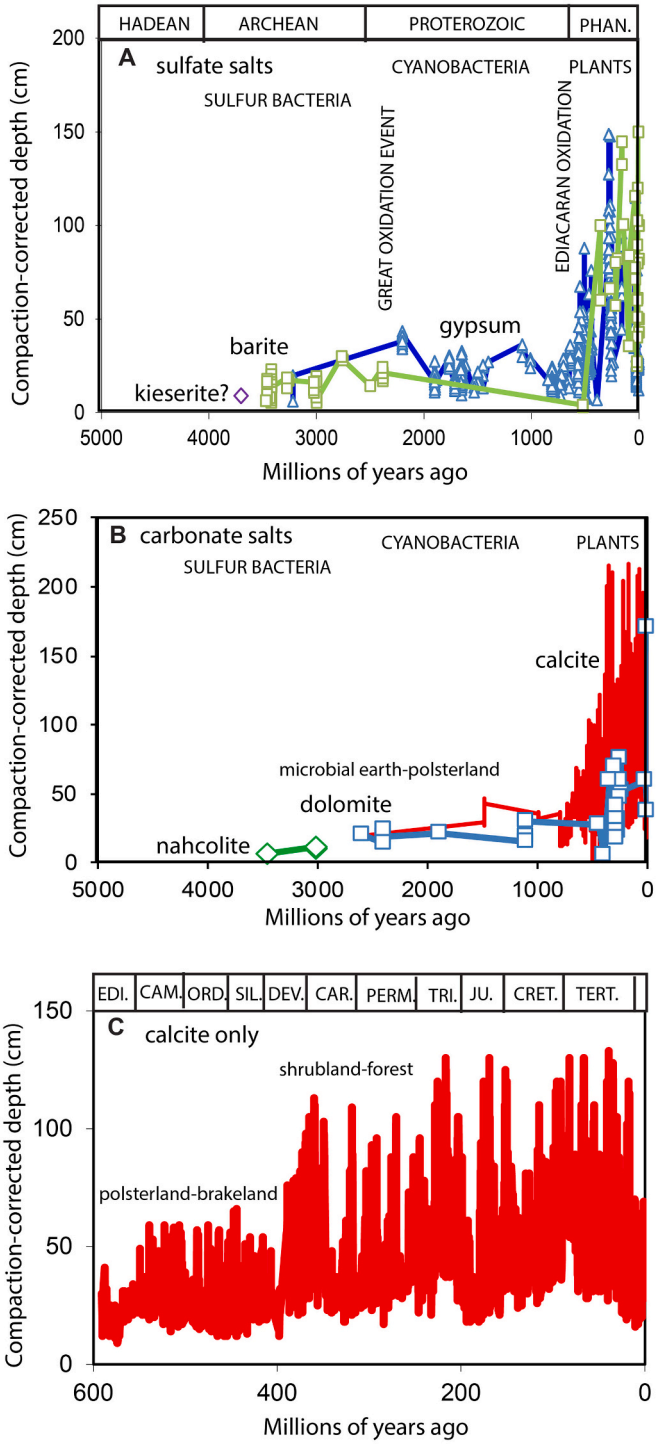

Fig. 6. Time series of compaction-corrected depth within paleosols to sulfate salts (A), and carbonate salts (B—C).

paleosols in Finland (Pekkarinen, 1979). The appearance of dolomite in soils marks a turn from acid-sulfate soils toward perineutral soil pH (Zhang et al., 2012). Pisolitic dolomite at the top of the 1850 Ma Mara Formation of Bathurst Inlet has also been regarded as a paleosol (Campbell and Cecile, 1981; Grotzinger et al., 1987).

The oldest pedogenic low-magnesium calcite known to me is only as old as 1460 Ma (Winston and Link, 1993) in Montana (Fig. 1A). Judging from comparable modern soils (Navarro-González et al., 2003; O'Brien et al., 2019), this may also mark a turn toward a diverse eukaryotic microbiome. Experimental studies have shown that dolomite rather than

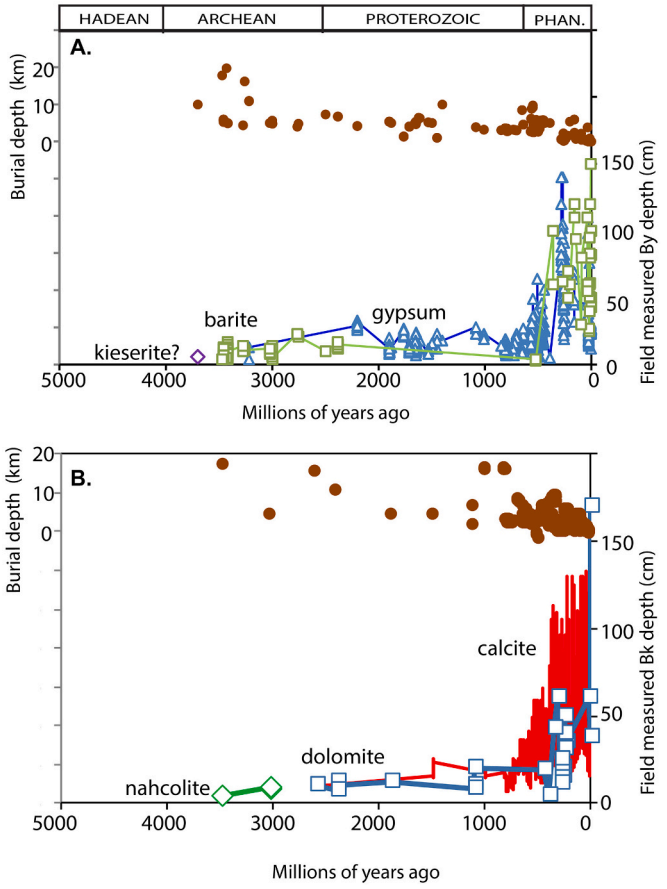

Fig. 7. Time series of raw field measurements of depth in paleosols to sulfate salts (A) and carbonate (B) with depth of burial by overburden. The overall pattern is similar to that of compaction-corrected data (Fig. 2).

calcite is favored by sugars from decay of extracellular polysaccharides. Galactose and rhamnose catalytic for dolomite are produced mainly by methanogens, fermenting bacteria and sulfur reducing bacteria under dysaerobic conditions. Glucose and mannose catalytic for calcite are produced by cyanobacteria, among others in well drained soils (Zhang et al., 2012). The geologically early appearance of dolomite in soils shortly after initial oxygenation of the 2450 Ma Great Oxidation Event, and its recurrence during Phanerozoic greenhouse CO_2 spikes, may have been due to transient soil anoxia and dysaerobic soil microbiomes (Kearsey et al., 2012). Conversely the transition from dolomite or sulfate paleosols toward calcite paleosols may reflect a shift to more highly oxidized soils under higher atmospheric oxygen during cooling to 720 Ma Neoproterozoic Snowball Earth (Retallack, 2021a; Retallack et al., 2021b).

6. Increasing salt depth in soils

Soil salts may be very common within subsurface horizons of nodules or sand crystals of carbonate (Bk horizon) or sulfate (By horizon) with a depth in the profile (Fig. 1) related to ppm soil CO_2 respired by the soil microbiome (Eqs. (2), (3) from Breecker and Retallack, 2014), and to tree height (Retallack and Huang, 2011), and both are proportional to mean annual precipitation (Retallack, 2005a). Soil salts are soluble in water, especially acidic water (Krumbein and Garrels, 1952). Productive ecosystems produce high soil CO_2 and the weak acid, carbonic acid (Breecker and Retallack, 2014). In contrast, oxidation of sulfide produces strong acid, sulfuric acid (Benison and Bowen, 2015). Compilation of depths below the truncated upper surface of paleosols to the salt horizons (Bk and By) shows stepwise increases through time (Fig. 5). This depth in sedimentary sequences is consistent within local sequences of paleosols, and paleosols beneath erosional sandstones and conglomerates were avoided (Retallack, 2011, 2013, Retallack, 2015). Original depth to salt horizons is needed for comparison with modern soil, but paleosols are variably compacted by overburden during burial. Known depth of burial inferred from regional stratigraphic thicknesses, or coalification, or metamorphic grade, has been used to calculate original depth to salts in the profile (Supplementary Information Table S1) using physical constants for Aridisols (Eq. (1) from Sheldon and Retallack, 2001). Data transformed for burial compaction (Fig. 6) shows increases through time comparable with raw data (Fig. 5), because burial depths did not vary greatly (Fig. 7).

Compaction-corrected depth to gypsic and calcic horizons can be used to calculate secondary soil productivity (ppm CO_2) from transfer functions (Eqs. (4), (5)) derived from late growing season soil CO_2 in modern aridland soils (Breecker and Retallack, 2014). The late growing season was chosen as it is at the end of a stable plateau of soil CO_2 between the unpredictable spring flush of productivity and very low levels in the dormant season. Levels of 2000 ppm are common in modern desert soils (Montañez, 2013), but soil respiration can be much higher in soils completely flushed of salts under humid temperate (4000–10,000 ppm: Montañez, 2013), and tropical forests (up to 104,000 ppm: Matsumoto et al., 1997).

Barite and gypsum were deeper in soils than calcite and dolomite within the same profiles during the past (Fig. 5), as they are still today (Retallack and Huang, 2010; Jennings and Driese, 2014). Shallow depths are evidence of low biological productivity in aridlands until the Ediacaran (549 Ma), when diverse biota appeared (Retallack, 2016). Ediacaran depths to salts and inferred soil productivity are not much different from Cambrian levels, but there is a peak during the Late Ordovician (447 Ma), coinciding with the rise of land plants (Retallack, 2015). The large increase in depth from Middle to Late Devonian (386–359 Ma) coincides with evolution and spread of trees (Retallack, 2011). The next step to deeper salts was during the Late Triassic (216 Ma) spread of broadleaf pteridosperms and gnetaleans, and perhaps ancestors of angiosperms (Herendeen et al., 2017). Increased vascular efficiency of angiosperm leaves and wood, and thus more voluminous transpiration, has also been proposed to have increased global humidity (Boyce and Leslie, 2012), and this would have driven salts deeper in soils. Increased penetration and exudates from roots also increased soil respiration and productivity (Algeo and Scheckler, 2010), with consequences for ocean anoxia and productivity (Algeo et al., 1995). The Phanerozoic record is dense enough to show also a series of greenhouse spikes induced by catastrophic bolide impacts and basaltic eruptions of large igneous provinces. These stand out in the Phanerozoic data used here, because they were chosen from particular regions with long sequences of calcareous paleosols ordered by superposition (Retallack, 2009). Randomly selected data would show great variance at all ages, but define similar plateaus.

7. Evolution of life and atmosphere

These new data quantify for aridlands biotic enhancement of weathering through time. Schwartzman (2017) proposed global biotic enhancement of weathering of a factor of 5–10 from Archean to Proterozoic, factor of 2–5 with early Paleozoic non-vascular land plants and factor of 10 after mid-Paleozoic trees for a total enhancement of 50 to offset 30% increase in solar energy with stellar evolution by greenhouse gas consumption. Archean to Paleoproterozoic paleosols demonstrate aggressive acid-sulfate weathering by sulfuric acid at pH 3–4 creating gypsic horizons (Retallack et al., 2016; Retallack, 2018), but perineutral hydrolytic weathering by carbonic acid also by microbial earth communities begins around Mesoproterozoic creating rare calcic horizons. Calcic soils remained rare until Neoproterozoic (Retallack, 2021b; Retallack et al., 2021a). Archean-Paleoproterozoic levels of 1500–2000 ppm late growing season CO_2 persisted until late Neoproterozic under

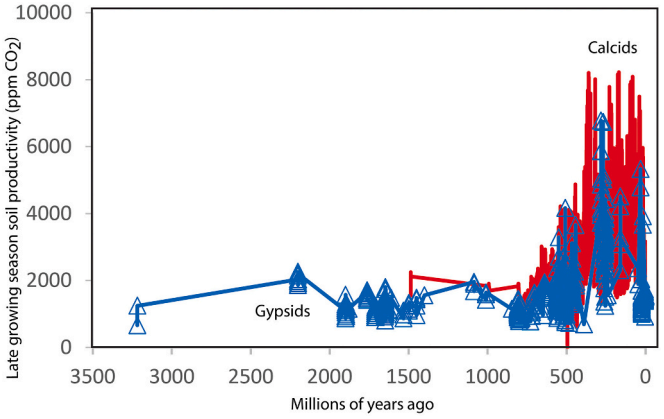

Fig. 8. Changing aridland soil productivity through time inferred from compaction-corrected depth to gypsic and calcic horizons in paleosols (Eqs. (1), (4–5)).

microbial earths, but then rose to 2000–5000 ppm under polsterlands (ground-hugging clumped vegetation: Retallack, 1992) of early non-vascular land plants, and later to almost 10,000 ppm under forests (Fig. 8). These figures match Schwartzman (2017) global estimates reasonably well, but only apply to aridlands of unknown global distribution. Other data from humid climate paleosols (Neaman et al., 2005; Beaty and Planavsky, 2020) and paleogeographic mapping of paleoclimate promise more accurate accounting of the progress of biotic enhancement of weathering in deep time.

The transition from gypsic to calcic paleosols around the time of the Great Oxidation Event (2460 Ma: Gumsley et al., 2017) may also be related to changing soil microbiomes, comparable with the gypsic to calcic soil transition in the Atacama Desert (Navarro-González et al., 2003; Neilson et al., 2017; Araya et al., 2020). Paleosol profiles have long been important proxies for atmospheric composition (Rye and Holland, 1990; Sheldon, 2006), independent of global greenhouse temperature models (Berner, 2006), sedimentary rock inventories (Kump, 2008), and marine geochemical proxies (Canfield and Farquhar, 2009). Terrestrial communities of anoxic purple sulfur bacteria in gypsic paleosols lived in an Archean low O_2 atmosphere (Retallack et al., 2016), terminated at the Great Oxidation Event, during appearance of carbonate paleosols of cyanobacteria (Figs. 2-3). Gains in atmospheric oxygen were consolidated with evolution of land plants and trees, and their deeper and more effective rhizospheres (Retallack and Huang, 2011; Retallack, 2015). The fossil record of salts in soils is thus a proxy for the coevolution of life and climate in dry regions, demonstrating changes confirmed by the independent record of non-calcareous paleosols of humid regions (Rye and Holland, 1990; Beaty and Planavsky, 2020).

The record of soil salts in deep time thus supports the conclusion of Hazen et al. (2008, p.1706) "minerals at Earth's surface have co-evolved with life. Indeed, most of Earth's mineral diversity today may be a consequence, direct or indirect, of the biosphere."

Declaration of Competing Interest

This is to certify that I, Gregory J. Retallack, have no known competing financial interests or personal relationships that could have appeared to influence the work reported in this paper.

Acknowledgments

Useful discussion came from Nathan Sheldon, Adrian Broz, David Krinsley, Tim Kearsey, Hiroshi Ohmoto, Neil Tabor, and Don Winston.

Appendix A. Supplementary data

Supplementary data to this article can be found online at https://doi.org/10.1016/j.palaeo.2022.111016.

References

Algeo, T.J., Scheckler, S.E., 2010. Land plant evolution and weathering rate changes in the Devonian. J. Earth Sci. 21, 75–78.
Algeo, T.J., Berner, R.A., Maynard, J.B., Scheckler, S.E., 1995. Late Devonian oceanic anoxic events and biotic crises:"rooted" in the evolution of vascular land plants. GSA Today 5 (3), 45–66.
Al-Kofahi, M.M., Hallak, A.B., Al-Juwair, H.A., Saafin, A.K., 1993. Analysis of desert rose using PIXE and RBS techniques. X-Ray Spectrom. 22, 23–27.
Anand, R.R., Paine, M., 2002. Regolith geology of the Yilgarn Craton, Western Australia: implications for exploration. Aust. J. Earth Sci. 49, 3–162.
Araya, J.P., González, M., Cardinale, M., Schnell, S., Stoll, A., 2020. Microbiome dynamics associated with the Atacama flowering desert. Front. Microbiol. 10, e3160.
Beaty, B.J., Planavsky, N.J., 2020. A 3 by record of a biotic influence on terrestrial weathering. Geology 49, 407–411.
Benison, K.C., Bowen, B.B., 2015. The evolution of end-member continental waters: the origin of acidity in southern Western Australia. GSA Today 25 (6), 4–10.
Benison, K.C., Goldstein, R.H., 2000. Sedimentology of ancient saline pans: an example from the Permian Opeche Shale, Williston Basin, North Dakota, USA. J. Sediment. Res. 70, 159–169.
Berner, R.A., 2006. GEOCARBSULF: a combined model for Phanerozoic atmospheric O_2 and CO_2. Geochim. Cosmochim. Acta 70, 5653–5664.
Bockheim, J.G., 2014. Soil Geography of the USA. Springer, Dordrecht, 320 p.
Boyce, C.K., Leslie, A.B., 2012. The paleontological context of angiosperm vegetative evolution. Int. J. Plant Sci. 173, 561–568.
Breecker, D.O., Retallack, G.J., 2014. Refining the pedogenic carbonate atmospheric CO_2 proxy and application to Miocene CO_2. Palaeogeogr. Palaeoclimatol. Palaeoecol. 406, 1–8.
Breecker, D.O., Sharp, Z.D., McFadden, L.D., 2009. Seasonal bias in the formation and stable isotopic composition of pedogenic carbonate in modern soils from Central New Mexico, USA. Geol. Soc. Am. Bull. 121, 630–640.
Broz, A., Retallack, G.J., Maxwell, T.M., Silva, L.C., 2021. A record of vapour pressure deficit preserved in wood and soil across biomes. Sci. Rep. 11, 1–12.
Buick, R., Dunlop, J.S.R., 1990. Evaporitic sediments of early Archaean age from the Warrawoona Group, North Pole, Western Australia. Sedimentology 37, 247–277.
Campbell, F.H.A., Cecile, M.P., 1981. Evolution of the early Proterozoic Kilohigok Basin, Bathurst Inlet-Victoria Island, North West Territories. In: Campbell, F.H.A. (Ed.), Proterozoic Basins of Canada, Geol. Soc. Canada Pap. 81-10, pp. 103–130.
Canfield, D.E., Farquhar, J., 2009. Animal evolution, bioturbation, and the sulfate concentration of the oceans. U.S. Nat. Acad. Sci. Proc. 106, 8123–8127.
Carson, C.D., Fanning, D.S., Dixon, J.B., 1982. Alfisols and Ultisols with acid sulfate weathering features in Texas. In: Kittick, J.A., Fanning, D.S., Hossner, L.R. (Eds.), Acid Sulfate Weathering, Soil Soc. Amer. Spec. Publ, vol. 10, pp. 127–146.
Crits-Christoph, A., Robinson, C.K., Barnum, T., Fricke, W.F., Davila, A.F., Jedynak, B., McKay, C.P., DiRuggiero, J., 2013. Colonization patterns of soil microbial communities in the Atacama Desert. Microbiome 1, 1–13.
Diaz, M.A., Li, J., Michalski, G., Darrah, T.H., Adams, B.J., Wall, D.H., Hogg, I.D., Fierer, N., Welch, S.A., Gardner, C.B., Lyons, W.B., 2020. Stable isotopes of nitrate, sulfate, and carbonate in soils from the Transantarctic Mountains, Antarctica: a record of atmospheric deposition and chemical weathering. Front. Earth Sci. https://doi.org/10.3389/feart.2020.00341/.
Dietrich, M., 1975. Wüstenrose. Verein. Freunde Mineral. Geol, 26, pp. 217–219.
Einaudi, M.T., Hedenquist, J.W., Inan, E.E., 2003. Sulfidation state of fluids in active and extinct hydrothermal systems: Transitions from porphyry to epithermal environments. In: Simmons, S.F., Graham, I. (Eds.), Volcanic, Geothermal, and Ore-Forming Fluids: Rulers and Witnesses of Processes within the Earth. Soc. Econ. Geol. Spec. Publ, vol. 10, pp. 285–314.
Ganzeveld, L., Lelieveld, J., Roelofs, G.J., 1998. A dry deposition parameterization for sulfur oxides in a chemistry and general circulation model. J. Geophys. Res.-Atmos. 103, 5679–5694.
Giordani, P., Modenesi, P., Tretiach, M., 2003. Determinant factors for the formation of the calcium oxalate minerals, weddellite and whewellite, on the surface of foliose lichens. Lichenologist 35, 255–270.
Grotzinger, J.P., McCormick, D.S., Pelechaty, S.M., 1987. Progress report on the stratigraphy, sedimentology and significance of the Kimerot and Bear Creek Groups, Kilohigok Basin, District of Mackenzie. Geol. Surv. Can. Pap. 87-lA, 219–238.
Gumsley, A.P., Chamberlain, K.R., Bleeker, W., Söderlund, U., de Kock, M.O., Larsson, E. R., Bekker, A., 2017. Timing and tempo of the Great Oxidation Event. Proc. U.S. Nat. Acad. Sci. 114, 1811–1816.
Harden, J.W., Taylor, E.M., Reheis, M.C., McFadden, L.D., 1991. Calcic, gypsic, and siliceous soil chronosequences in arid and semiarid environments. In: Nettleton, W. D. (Ed.), Occurrence, Characteristics, and Genesis of Carbonate, Gypsum, and Silica Accumulations in Soils, Soil Sci. Soc. Amer. Spec. Publ, vol. 26, pp. 1–16.
Hazen, R.M., Papineau, D., Bleeker, W., Downs, R.T., Ferry, J.M., McCoy, T.J., Sverjensky, D.A., Yang, H., 2008. Mineral evolution. Am. Mineral. 93, 1693–1720.
Herendeen, P.S., Friis, E.M., Pedersen, K.R., Crane, P.R., 2017. Palaeobotanical redux: revisiting the age of the angiosperms. Nat. Plant 3 (e17015), 1–8.
Howari, F.M., Goodell, P.C., Miyamoto, S., 2002. Spectral properties of salt crusts formed on saline soils. J. Environ. Qual. 31 (5), 1453–1461.

Jennings, D.S., Driese, S.G., 2014. Understanding barite and gypsum precipitation in upland acid-sulfate soils: an example from a Lufkin Series toposequence, south-central Texas, USA. Sediment. Geol. 299, 106–118.
Jones, B., 2017. Review of aragonite and calcite crystal morphogenesis in thermal spring systems. Sediment. Geol. 354, 9–23.
Kearsey, T., Twitchett, R.J., Newell, A.J., 2012. The origin and significance of pedogenic dolomite from the Upper Permian of the South Urals of Russia. Geol. Mag. 149, 291–307.
Krumbein, W.C., Garrels, R.M., 1952. Origin and classification of chemical sediments in terms of pH and oxidation-reduction potentials. J. Geol. 60, 1–33.
Kump, L.R., 2008. The rise of atmospheric oxygen. Nature 451, 277–278.
Lock, B.E., 2002. Sabkhas ancient and modern. Trans. Gulf Coast Assoc. Geol. Soc. 52, 645–657.
Lowe, D.R., Worrell, G.F., 1999. Sedimentology, mineralogy, and implications of silicified evaporites in the Kromberg Formation, Barberton Greenstone Belt, South Africa. In: Lowe, D.R., Byerly, G.R. (Eds.), Geologic Evolution of the Barberton Greenstone Belt South Africa, Spec. Pap. Geol. Soc. Amer, vol. 329, pp. 167–188.
Lowenstein, T.K., Jagniecki, E.A., Carroll, A.R., Smith, M.E., Renaut, R.W., Owen, R.B., 2017. The Green River salt mystery: what was the source of the hyperalkaline lake waters? Earth Sci. Rev. 173, 295–306.
Matsumoto, E., Naruoka, T., da Silva, E.F., 1997. Concentration of carbon dioxide in regolith air in different tropical geoecosystems of Northeast Brazil. Inst. Geosci.Univ. Tsukuba Ann. Rept. 23, 11–15.
Mees, F., Tursina, T.V., 2018. Salt minerals in saline soils and salt crusts. Interpretation of micromorphological features of soils and regoliths. In: Stoops, G., Marcelino, V., Mees, F. (Eds.), Interpretation of Micromorphological Features of Soils and Regoliths. Elsevier, Amsterdam, pp. 289–321.
Monger, H.C., Daugherty, L.A., Lindemann, W.C., Liddell, C.M., 1991. Microbial precipitation of pedogenic calcite. Geology 19, 997–1000.
Montañez, I.P., 2013. Modern soil system constraints on reconstructing deep-time atmospheric CO_2. Geochim. Cosmochim. Acta 101, 57–75.
Mormile, M.R., Hong, B.Y., Benison, K.C., 2009. Molecular analysis of the microbial communities of Mars analog lakes in Western Australia. Astrobiology 9, 919–930.
Nabhan, S., Luber, T., Scheffler, F., Heubeck, C., 2016. Climatic and geochemical implications of Archean pedogenic gypsum in the Moodies Group (~ 3.2 Ga), Barberton Greenstone Belt, South Africa. Precambrian Res. 275, 119–134.
Navarro-González, R., Rainey, F.A., Molina, P., Bagaley, D.R., Hollen, B.J., de la Rosa, J., Small, A.M., Quinn, R.C., Grunthaner, F.J., Cáceres, L., Gomez-Silva, B., 2003. Mars-like soils in the Atacama Desert, Chile, and the dry limit of microbial life. Science 302, 1018–1021.
Neaman, A., Chorover, J., Brantley, S.L., 2005. Element mobility patterns record organic ligands in soils on early Earth. Geology 33, 117–120.
Neilson, J.W., Califf, K., Cardona, C., Copeland, A., Van Treuren, W., Josephson, K.L., Knight, R., Gilbert, J.A., Quade, J., Caporaso, J.G., Maier, R.M., 2017. Significant impacts of increasing aridity on the arid soil microbiome. MSystems 2 e00195–16.
O'Brien, F.J.M., Almaraz, M., Foster, M., Hill, A., Huber, D., King, E., Langford, H., Lowe, M.A., Mickan, B.S., Miller, V., Moore, O., 2019. Soil salinity and pH drive soil bacterial community composition and diversity along a lateritic slope in the Avon River Critical Zone Observatory, Western Australia. Front. Microbiol. 10, 1–19.
Otálora, F., Mazurier, A., Garcia-Ruiz, J.M., Van Kranendonk, M.J., Kotopoulou, E., El Albani, A., Garrido, C.J., 2018. A crystallographic study of crystalline casts and pseudomorphs from the 3.5 Ga Dresser Formation, Pilbara Craton (Australia). J. Appl. Crystallogr. 51, 1050–1058.
Pekkarinen, L.J., 1979. The Karelian formations and their depositional basement in the Kiihetelysvaar-Värtsilä area, East Finland. Geol. Surv. Finland Bull. 301, 1–141.
Quade, J., Rech, J.A., Latorre, C., Betancourt, J.L., Gleeson, E., Kalin, M.T., 2007. Soils at the hyperarid margin: the isotopic composition of soil carbonate from the Atacama Desert, Northern Chile. Geochim. Cosmochim. Acta 71, 3772–3795.
Retallack, G.J., 1983. Late Eocene and Oligocene paleosols from Badlands National Park, South Dakota. Geol. Soc. Am. Spec. Pap. 193, 1–82.
Retallack, G.J., 1991. Miocene Paleosols and Ape Habitats of Pakistan and Kenya. Oxford Univ, New York, p. 246.
Retallack, G.J., 1992. What to call early plant formations on land. Palaios 7, 508–520.
Retallack, G.J., 2005a. Pedogenic carbonate proxies for amount and seasonality of precipitation in paleosols. Geology 33, 333–336.
Retallack, G.J., 2005b. Permian greenhouse crises. In: Lucas, S.G. (Ed.), The Nonmarine Permian. New Mexico Mus. Nat. Hist. Sci. Bull, vol. 30, pp. 256–269.
Retallack, G.J., 2009. Greenhouse crises of the past 300 million years. Geol. Soc. Am. Bull. 121, 1441–1455.
Retallack, G.J., 2011. Woodland hypothesis for Devonian evolution of tetrapods. J. Geol. 119, 235–258.
Retallack, G.J., 2013. Ediacaran life on land. Nature 493, 89–92.
Retallack, G.J., 2014. Paleosols and paleoenvironments of early Mars. Geology 42, 755–758.
Retallack, G.J., 2015. Late Ordovician glaciation initiated by early land plant evolution, and punctuated by greenhouse mass-extinctions. J. Geol. 123, 509–538.
Retallack, G.J., 2016. Field and laboratory tests for recognition of Ediacaran paleosols. Gondwana Res. 36, 94–110.
Retallack, G.J., 2018. Oldest recognized paleosols on Earth, Panorama Formation (3.46 Ga), Western Australia. Palaeogeogr. Palaeoclimatol. Palaeoecol. 489, 230–248.
Retallack, G.J., 2019. Soils of the Past. Wiley, Chichester, p. 534.
Retallack, G.J., 2020. Zebra rock and other Ediacaran paleosols from Western Australia. Aust. J. Earth Sci. 68, 532–556.
Retallack, G.J., 2021a. Multiple Permian-Triassic life crises on land and at sea. Glob. Planet. Chang. 198, 103415.
Retallack, G.J., 2021b. Paleosols and weathering leading up to Snowball Earth in Central Australia. Aust. J. Earth Sci. 68, 1122–1148.
Retallack, G.J., 2022. Ordovician-Devonian lichen canopies before evolution of woody trees. Gondwana Res. 106, 211–223.
Retallack, G.J., Huang, C.-M., 2010. Depth to gypsic horizon as a proxy for paleoprecipitation in paleosols of sedimentary environments. Geology 38, 403–406.
Retallack, G.J., Huang, C., 2011. Ecology and evolution of Devonian trees in New York, USA. Palaeogeogr. Palaeoclimatol. Palaeoecol. 299, 110–128.
Retallack, G.J., Mao, X., 2019. Paleoproterozoic (ca. 1.9 Ga) megascopic life on land in Western Australia. Palaeogeogr. Palaeoclimatol. Palaeoecol. 532, 109266.
Retallack, G.J., Noffke, N., 2019. Are there ancient soils in the 3.7 Ga Isua Greenstone Belt, Greenland? Palaeogeogr. Palaeoclimatol. Palaeoecol. 514, 18–30.
Retallack, G.J., Bestland, E.A., Fremd, T.J., 1999. Eocene and Oligocene paleosols of Central Oregon. Geol. Soc. Am. Spec. Pap. 344, 1–196.
Retallack, G.J., Tanaka, S., Tate, T., 2002. Late Miocene advent of tall grassland paleosols in Oregon. Palaeogeogr. Palaeoclimatol. Palaeoecol. 183, 329–354.
Retallack, G.J., Wynn, J.G., Fremd, T.J., 2004. Glacial-interglacial–scale paleoclimatic change without large ice sheets in the Oligocene of Central Oregon. Geology 32, 297–300.
Retallack, G.J., Gose, B.N., Osterhout, J.T., 2015. Periglacial paleosols and Cryogenian paleoclimate near Adelaide, South Australia. Precambrian Res. 263, 1–18.
Retallack, G.J., Krinsley, D.H., Fischer, R., Razink, J.J., Langworthy, K.A., 2016. Archean coastal-plain paleosols and life on land. Gondwana Res. 40, 1–20.
Retallack, G.J., Broz, A.P., Lai, L.S.H., Gardner, K., 2021a. Neoproterozoic marine chemostratigraphy, or eustatic sea level change? Palaeogeogr. Palaeoclimatol. Palaeoecol. 562, 110155.
Retallack, G.J., Chen, Z.Q., Huang, Y., Fang, Y., 2021b. Oxidizing atmosphere and life on land during the late Paleoproterozoic outset of the "boring billion". Precambrian Res. 364, 106361.
Royer, D.L., 1999. Depth to pedogenic carbonate horizon as a paleoprecipitation indicator? Geology 27, 1123–1126.
Rye, R., Holland, H.D., 1990. Paleosols and the evolution of atmospheric oxygen: a critical review. Am. J. Sci. 298, 621–672.
Schlesinger, W.H., 1985. The formation of caliche in soils of the Mojave Desert, California. Geochim. Cosmochim. Acta 49, 57–66.
Schwartzman, D.G., 2017. Life's critical role in the long-term carbon cycle: biotic enhancement of weathering. AIMS Geosci. 3 (2), 216–238.
Sheldon, N.D., 2006. Precambrian paleosols and atmospheric CO_2 levels. Precambrian Res. 147, 148–155.
Sheldon, N.D., Retallack, G.J., 2001. Equation for compaction of paleosols due to burial. Geology 29, 247–250.
Sheldon, N.D., Retallack, G.J., Tanaka, S., 2002. Geochemical climofunctions from North American soils and application to paleosols across the Eocene-Oligocene boundary in Oregon. J. Geol. 110, 687–696.
Smykatz-Kloss, W., Roy, P.D., 2010. Evaporite mineralogy and major element geochemistry as tools for palaeoclimatic investigations in arid regions: a synthesis. Bol. Soc. Geol. Mex. 62, 379–390.
Stefano, L., Vinicio, M., Marco, R., Charlotte, S.B., 2010. The primary lower Gypsum in the Mediterranean: a new facies interpretation for the first stage of the Messinian salinity crisis. Palaeogeogr. Palaeoclimatol. Palaeoecol. 297, 83–99.
Stoker, C.R., Clarke, J., Direito, S.O., Blake, D., Martin, K.R., Zavaleta, J., Foing, B., 2011. Mineralogical, chemical, organic and microbial properties of subsurface soil cores from Mars Desert Research Station (Utah, USA): phyllosilicate and sulfate analogues to Mars mission landing sites. Int. J. Astrobiol. 10, 269–289.
Sugahara, H., Sugitani, K., Mimura, K., Yamashita, F., Yamamoto, K., 2010. A systematic rare-earth elements and yttrium study of Archean cherts at the Mount Goldsworthy greenstone belt in the Pilbara Craton: implications for the origin of microfossil-bearing black cherts. Precambrian Res. 177, 73–87.
Traveria, A., Amigó, J.M., Montoriol-Pous, J., 1971. Nota sobre una masa de "rosas del desierto" recogida en el Gran Erg oriental (Argelia). Acta Geol. Hisp. 6, 49–52.
Vítek, P., Cámara-Gallego, B., Edwards, H.G., Jehlička, J., Ascaso, C., Wierzchos, J., 2013. Phototrophic community in gypsum crust from the Atacama Desert studied by Raman spectroscopy and microscopic imaging. Geomicrobiol J. 30, 399–410.
Wang, X., Hua, T., Zhang, C., Lang, L., Wang, H., 2012. Aeolian salts in Gobi deserts of the western region of Inner Mongolia: gone with the dust aerosols. Atmos. Res. 118, 1–9.
Watanabe, Y., Stewart, B.W., Ohmoto, H., 2004. Organic-and carbonate-rich soil formation~ 2.6 billion years ago at Schagen, East Transvaal district, South Africa. Geochim. Cosmochim. Acta 68, 2129–2151.
Whittig, L.D., Janitzky, P., 1963. Mechanisms of formation of sodium carbonate in soils: I. Manifestations of biological conversions. J. Soil Sci. 14, 322–333.
Winston, D., Link, P.K., 1993. Middle Proterozoic rocks of Montana, Idaho and eastern Washington: The Belt Supergroup. In: Reed, J.C., Bickford, M.E., Houston, R.S., Link, P.K., Rankin, D.W., Sims, P.K., Van Schmus, W.R. (Eds.), Precambrian Conterminous US. Geological Society of America, Boulder.
Zhang, F., Xu, H., Konishi, H., Shelobolina, E.S., Roden, E.E., 2012. Polysaccharide-catalyzed nucleation and growth of disordered dolomite: a potential precursor of sedimentary dolomite. Am. Mineral. 97, 556–567.
Ziegenbalg, S.B., Brunner, B., Rouchy, J.M., Birgel, D., Pierre, C., Böttcher, M.E., Caruso, A., Immenhauser, A., Peckmann, J., 2010. Formation of secondary carbonates and native sulphur in sulphate-rich Messinian strata, Sicily. Sediment. Geol. 227, 37–50.